Journal of Molecular Spectroscopy 259 (2010) 1–10

Contents lists available at ScienceDirect

Journal of Molecular Spectroscopy

journal homepage: www.elsevier.com/locate/jms

Rovibrational spectroscopy of the Fermi-interacting $v_4 = 1$ and $v_3 = v_6 = 1$ levels of DCF_3

Petr Pracna [a,*], Adina Ceausu-Velcescu [b], Adriana Predoi-Cross [c], Štěpán Urban [d]

[a] *J. Heyrovský Institute of Physical Chemistry, v.v.i., Academy of Sciences of the Czech Republic, Dolejškova 3, 18223 Prague, Czech Republic*
[b] *Université de Perpignan, Laboratoire de Mathématiques, Physique et Systèmes, 52 Avenue Paul Alduy, 66860 Perpignan Cedex, France*
[c] *University of Lethbridge, Department of Physics and Astronomy, 4401 University Drive, Lethbridge, AB, Canada T1K 3M4*
[d] *Department of Analytical Chemistry, Institute of Chemical Technology, 16628 Prague 6, Czech Republic*

ARTICLE INFO

Article history:
Received 3 July 2009
In revised form 22 September 2009
Available online 7 October 2009

Keywords:
Deuterated fluoroform
High-resolution IR spectroscopy
Anharmonic and vibration–rotation resonances

ABSTRACT

The high-resolution infrared spectrum of deuterated fluoroform (DCF_3) was studied in the 700 and 1200 cm^{-1} regions, with the aim of assigning and analyzing the v_4 CF_3 asymmetric stretching vibration. The Fermi-type anharmonic coupling between the $v_4 = 1$ and $v_3 = v_6 = 1$ rovibrational levels, already mentioned in an early work of Ruoff et al. [Spectrochimica Acta Part A 31A (1975) 1099–1100], was studied here for the first time under high resolution. Assignments in the $v_3 + v_6/v_4$ band system were confirmed and extended by the identification of the $v_3 + v_6 - v_6$ and $v_4–v_6$ bands in the 700 cm^{-1} region, the latter being enhanced near the Fermi crossings of the studied levels. Data from both the hot and difference bands were included in the analysis. The close separation of the studied vibrational levels of about 14.8 cm^{-1} produces a large variety of resonance crossings which involve levels with $\Delta k = 0, \ldots, 6$. Besides the Fermi ($\Delta k = 0$, $\Delta l = 0$) and Coriolis ($\Delta k = \pm 1$, $\Delta l = \mp 2$) resonances, they were accounted for by inclusion of additional higher-order ($\Delta k = \pm 2$, $\Delta l = \pm 2$ and $\Delta k = \pm 3$, $\Delta l = 0$) interaction terms between the vibrational states. The least-squares fit of more that 16,000 vibration-rotation transitions provides a quantitative reproduction of data in all bands.

1. Introduction

The present investigation of the $v_4 = 1$ and $v_3 = v_6 = 1$ rovibrational levels concludes the high-resolution studies of the six fundamental bands of the DCF_3 molecule, which have been carried out during approximately the last 15 years. The systematic investigation by high-resolution infrared and submillimeter wave (SMMW) spectroscopy has been undertaken, together with the HCF_3 molecule, in order to provide accurate information for the determination of the anharmonic potential function and equilibrium structure of fluoroform. A survey of the most recent studies of the DCF_3 molecule can be found e.g. in Ref. [1], and the most recent determination of the force field in Ref. [2]. Ref. [1] provides a reassignment of the v_6 fundamental band, together with the first high-resolution study of the $v_6 = 2$ $(A_1 + E)$ overtone level. It also includes a very accurate determination of all ground state rotational constants, including the axial ones, up to the sixth order.

Prior to this period, the only high-resolution study was done more than 20 years ago for the $v_1 = 1$ fundamental level by Dübal et al. [3]. Otherwise, only the low-resolution infrared studies by Ruoff et al. [4] and Fyke et al. [5] dating back to the 70 s and a microwave study from 1962 by Costain [6] were available. The latter three papers were the only source of experimental information on the rovibrational levels studied here. The rotational structure of these two IR bands was not resolved at that time, but the Fermi resonance between the $v_4 = 1$ and $v_3 = v_6 = 1$ levels could be analyzed by means of a band contour simulation. Since then this issue remained untouched, mainly because of the strongly congested spectrum and the complicated resonance patterns, which prevented accomplishing a quantitative reproduction of rovibrational data even with the Fermi resonance taken into account. The two rovibrational states form a kind of a 'twin' level system, in which various types of higher-order $\Delta(k - l) = 0, 3,$ and 6 vibration-rotation interactions, conventionally taken as perturbations within degenerate vibrational levels of symmetric top molecules, become important as intervibrational couplings involved in local resonant crossings. They therefore have to be included in the effective rovibrational Hamiltonian, besides the most prominent Fermi resonance.

As the information on all fundamental levels of the DCF_3 molecule has been made complete here, we have collected the basic information and literature references in a concise form in Table 1. Except for the present case of the $v_4 = 1$ level, all other fundamental vibrational levels have been treated as isolated because of considerable separations from the neighboring vibrational states, as can be seen from the graphical representation of vibrational energies

---

* Corresponding author. Fax: +420 286 582 307.
E-mail address: pracna@jh-inst.cas.cz (P. Pracna).

0022-2852/$ - see front matter © 2009 Elsevier Inc. All rights reserved.
doi:10.1016/j.jms.2009.09.007

Table 1
Basic characteristics of fundamental levels of DCF_3.

Mode	Approximate description	ν_i (cm^{-1})	α_i^B (10^{-3} cm^{-1})	α_i^C (10^{-3} cm^{-1})	IR	rot	References
ν_1 (A_1)	CD stretching	2261.3	1.347	0.162	✓	–	[3]
ν_2 (A_1)	CF_3 symmetric stretching	1111.2	1.851	0.462	✓	✓	[7,8]
ν_3 (A_1)	CF_3 symmetric deformation	694.3	0.688	0.147	✓	✓	[7,8]
ν_4 (E)	CF_3 asymmetric stretching	1211.2	0.425	0.514	✓	–	Present work
ν_5 (E)	CD rocking	975.4	0.314	0.009	✓	✓	[9]
ν_6 (E)	CF_3 asymmetric deformation	502.6	−0.066	0.363	✓	✓	[1,10]

up to the highest fundamental vibrational level $\nu_1 = 1$ in Fig. 1. The latter, however, falls into a cluster of levels around 2200 cm^{-1} for which only one other band at 2152 cm^{-1} was observed and tentatively assigned as the $2\nu_2$ overtone [3]. There still remain unexplained discrepancies between the expected and observed effective rotational constants of these two states, which are obviously due to analyzing them in the approximation of isolated levels. Their quantitative analysis will require not only considering the effect of the Fermi resonance between them, but also inclusion of additional neighboring vibrational levels with anharmonic and various types of vibration-rotation interactions. The present study may contribute valuable information to better representation of this cluster of interacting vibrational levels.

2. Experimental details

Five high-resolution FTIR spectra were used in this work. The details concerning the recording of the spectra are summarized in Table 2. Spectra A, B, C, and D were recorded in Wuppertal, using a Bruker IFS 120HR interferometer. The ν_4 and $\nu_3 + \nu_6$ bands were first studied from spectrum A. In order to reach higher J and K transitions of the ν_4 band, spectra B and C, both recorded at room temperature, were used. In order to improve our knowledge of the $\nu_3 = \nu_6 = 1$ and $\nu_4 = 1$ levels, not only through the corresponding combination and fundamental bands, but also using additional information from hot bands, spectrum D was employed, recorded also at room temperature. Calibration of these spectra was done using residual water lines as given in Ref. [11]. Wavenumber precision and accuracy were 2×10^{-4} and 5×10^{-4} cm^{-1}, respectively.

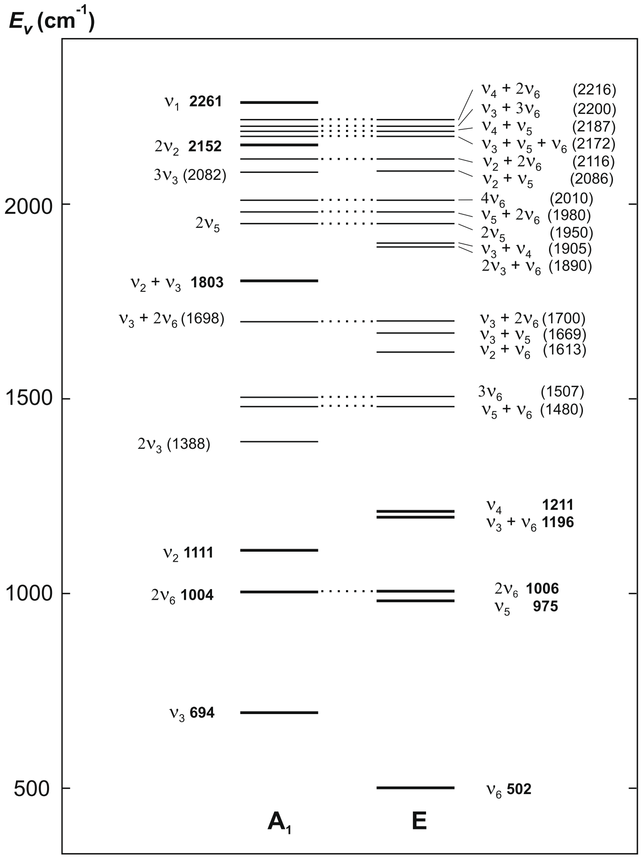

Fig. 1. Diagram of vibrational levels of DCF_3 up to the highest energy fundamental level $\nu_1 = 1$, separated to non-degenerate (A_1) and degenerate (E) levels. Overtone and combination levels having sublevels of both symmetries are drawn in both stacks and are connected with dotted lines. The levels analyzed so far are highlighted with bold lines and fonts. The energies of overtone and combination levels given in parentheses are estimated without including anharmonic corrections.

As spectrum D often presents very strong, almost saturated and rather broad lines, we recorded a second, lower pressure and higher path length spectrum in the 700 cm^{-1} region. Spectrum E was recorded at the Canadian Light Source in Saskatoon using a Bruker IFS 125HR interferometer. The wavenumber scale calibration was done using CO_2 lines in the 650 cm^{-1} region, as given in the HITRAN database [12]. The precision and accuracy of the measured transitions was estimated to be 1×10^{-4} and 3×10^{-4} cm^{-1}, respectively.

It has been pointed out in Ref. [1] that, when combining spectra from two different regions, their simultaneous analysis may reveal a slight inconsistency of their absolute wavenumber calibration. A small discrepancy of calibration between the two regions of FT spectra could indeed be observed when the data from the hot bands were temporarily given zero weights in the fits. The calibration inconsistency of about -6.4×10^{-5} cm^{-1} was removed by applying a post-calibration multiplication of wavenumbers in the 700 cm^{-1} region, shifting them upwards by this amount.

3. Description of the spectra and assignments

3.1. The ν_4/$\nu_3 + \nu_6$ bands

The two bands are strongly overlapped, with band origins separated by about 22 cm^{-1}. The highly congested spectrum shown in Fig. 2 hides most of the typical Q-branch patterns of perpendicular bands, which are usually the key to straightforward assignments in less crowded spectra. The prominent $^rQ_0$ branches of both bands can be visually identified in the overview spectrum near 1192.8 and 1214.4 cm^{-1} and correspond to the band structure known from the low-resolution studies [4,5]. The $^rQ_0$ branch of the stronger ν_4 band at 1214 cm^{-1}, shown in detail in Fig. 3a, has the J-spacing of lines very similar to the neighboring $^rQ_1$ and $^pQ_1$ branches, which suggests that the value of the l-type term is quite small ($q_{22}^4 << \alpha_B^4$), since it sums directly with $\alpha_B^4 = B_0 - B_4$ only in the $^rQ_0$ branch. The positive value of α_B^4 makes all the Q-branches degraded towards lower wavenumbers. The ^pQ_K branches which extend towards higher wavenumbers have quite regular spacing of about 0.55 cm^{-1} as they are less affected by the Fermi resonance. For the several lowest values of K they have the appearance of a textbook example of an unperturbed perpendicular band. The ^rQ_K branches, on the other hand, display a very irregular behavior in the vicinity of the Fermi resonance crossing. They are thus much less conspicuous and, in addition to this, positions of their individ-

Table 2
Experimental details of Fourier transform spectra used in this study.

Spectrum	A	B	C	D	E
Range (cm^{-1})	850–1500	850–1500	850–1500	400–880	520–800
Detector	MCT 800	MCT 800	MCT 800	Cu: Ge	Cu: Ge
Beamsplitter	KBr	KBr	KBr	KBr	KBr
No. of scans	280	80	360	340	200
Resolution[a] (cm^{-1})	0.0023	0.0024	0.0024	0.0024	0.0010
Path length (m)	0.2	9.6	9.6	9.6	24
Pressure (Pa)	250	20	250	250	100
Temperature (K)	228	293	293	293	293

[a] The resolution of the Bruker FTS was calculated as 0.9/MOPD, where MOPD is maximum optical path difference.

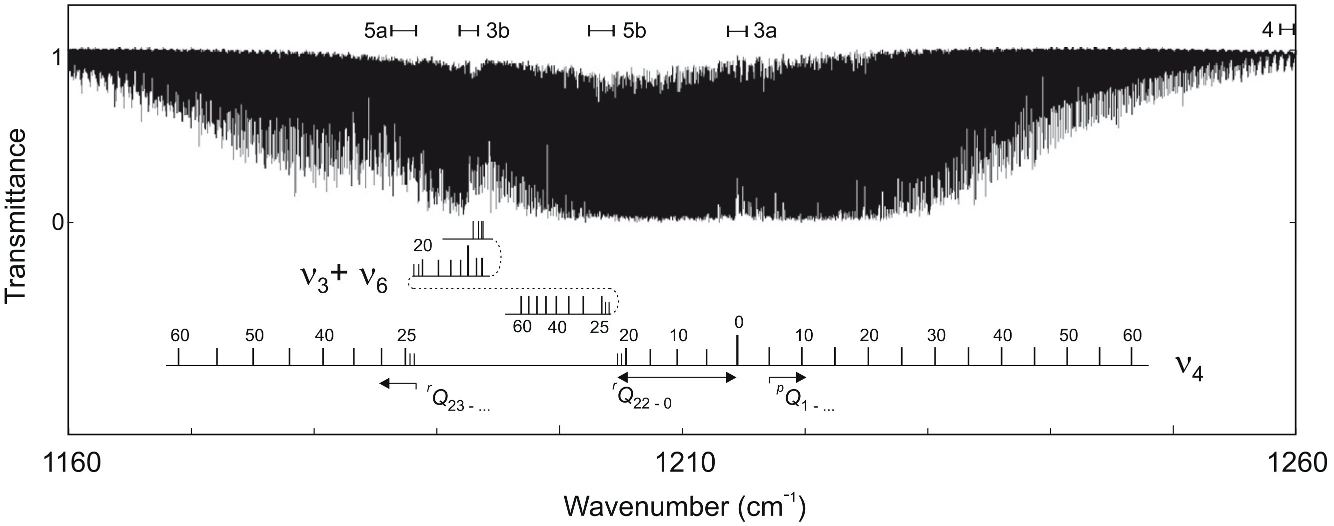

Fig. 2. Overview spectrum of the region of the ν_4 and $\nu_3+\nu_6$ bands of DCF$_3$. (spectrum A, cf. Table 2). Positions (heads) of the ${}^rQ_0$ branches of both bands are indicated by the longest ticks in the assignment combs. Positions of the ${}^pQ_K$ and ${}^rQ_K$ branches of both bands are indicated by ticks with steps of $K = 5n$, except the region of the Fermi crossing where all $K = 21$–24 are marked with the shortest ticks. The intervals above the spectrum refer to the spectrum sections shown in further figures with the corresponding numbers.

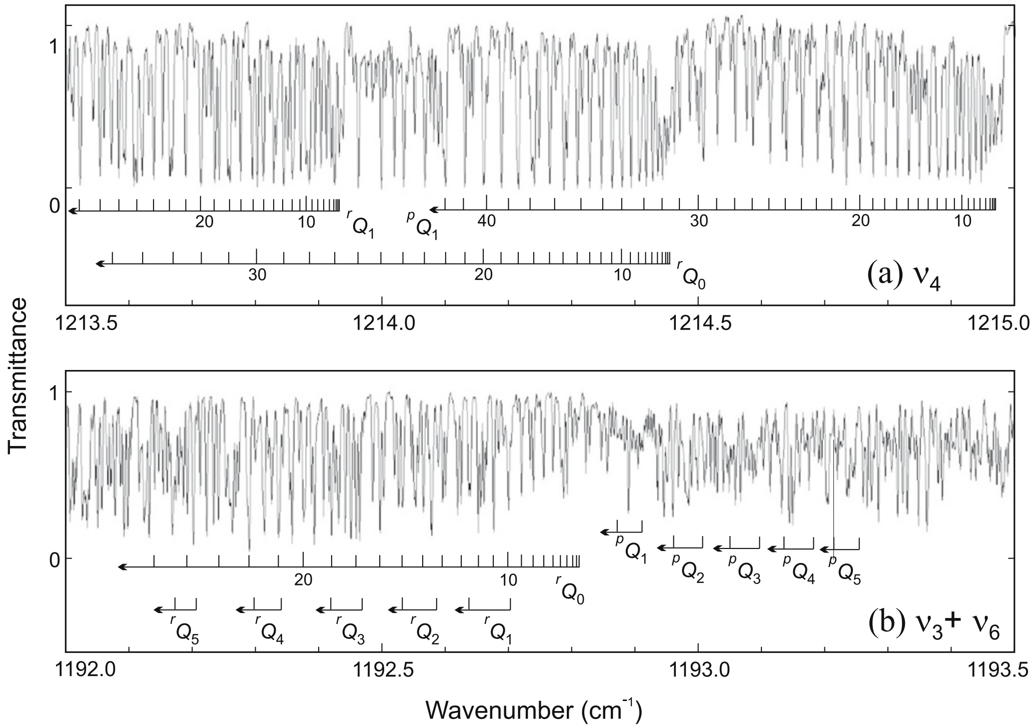

Fig. 3. (a) Detail of the spectrum A in the region of the ${}^rQ_0$, ${}^rQ_1$, and ${}^pQ_1$ branches of the ν_4 band with the assignment combs indicating some of the values of J. (b) Detail of the spectrum around the origin of the $\nu_3+\nu_6$ band showing the ${}^rQ_0$ branch and some of the low-K ${}^pQ_K$ and ${}^rQ_K$ branches, where ticks on their assignment combs indicate their origin and position of the $J = 10$ lines. Experimental conditions same as in Fig. 2.

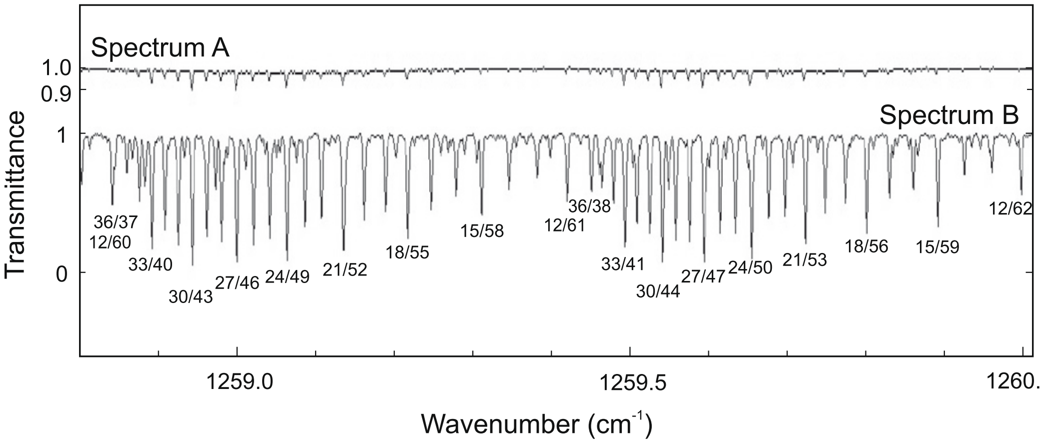

Fig. 4. Detail of the spectrum showing two clusters of the lines $^pR_K(J)$, $^pR_{K-1}(J+1)$, $^pR_{K-2}(J+2)$, ... with some of the K/J assignments indicated. The upper trace corresponds to spectrum A, the lower trace to spectrum B measured with lower pressure but longer path length.

ual lines are very often perturbed by overlaps with the structures of the $\nu_3 + \nu_6$ band. Therefore the assignments are much more reliable in the corresponding P and R branches.

For assigning the high$-K$ $\Delta K = -1$ transitions in the ν_4 band, we used the nice clusters of ^pR_K lines on the high wavenumber side of the band, shown in Fig. 4, where there is very little interference with other transitions. Such compact clusters are formed because of the small value of $(C - C\zeta)_4 \approx 0.021$ cm^{-1}, which puts the transitions $^pR_K(J)$, $^pR_{K-1}(J+1)$, $^pR_{K-2}(J+2)$, ... close together. We were of course able to find the corresponding ^pP and ^pQ branches for lower state combination difference checking (LSCD) using the Loomis-Wood for Windows (LWW) program package [13], but these fall into very congested regions of the spectra where the line positions are often strongly perturbed. Employing the spectra B and C with the path length of 9.6 m, we were able to extend assignments in the ^pR branches up to $J'/K' = 88/70$. On the $\Delta K = +1$ side of the ν_4 band we could assign transitions in the ^rQ and ^rR branches up to $J'/K' = 75/50$.

The separations of the Q-branches in the $\nu_3 + \nu_6$ perpendicular band are considerably smaller than in the ν_4 band and this makes the region around the band origin quite congested (Fig. 3b). They become larger, however, for the ^rQ_K branches with the Fermi coupling growing and displacing them more and more towards lower wavenumbers for $K' \cdot l < 24$, i.e. before the resonant crossing occurs. For $K' \cdot l \geqslant 24$ they are pushed up to higher wavenumbers by about 16 cm^{-1}, i.e. about twice the value of the Fermi resonance term (Fig. 5). For $K' \cdot l > 40$, with the Fermi coupling progressively weakening, the regular spacing of the ^rQ_K branches is restored. The positions of the ^pQ_K branches are perturbed much less by the Fermi interaction and thus resemble much more the structure of the ν_6 band. The $^rQ_0$ branch of the $\nu_3 + \nu_6$ band has the J-spacing very

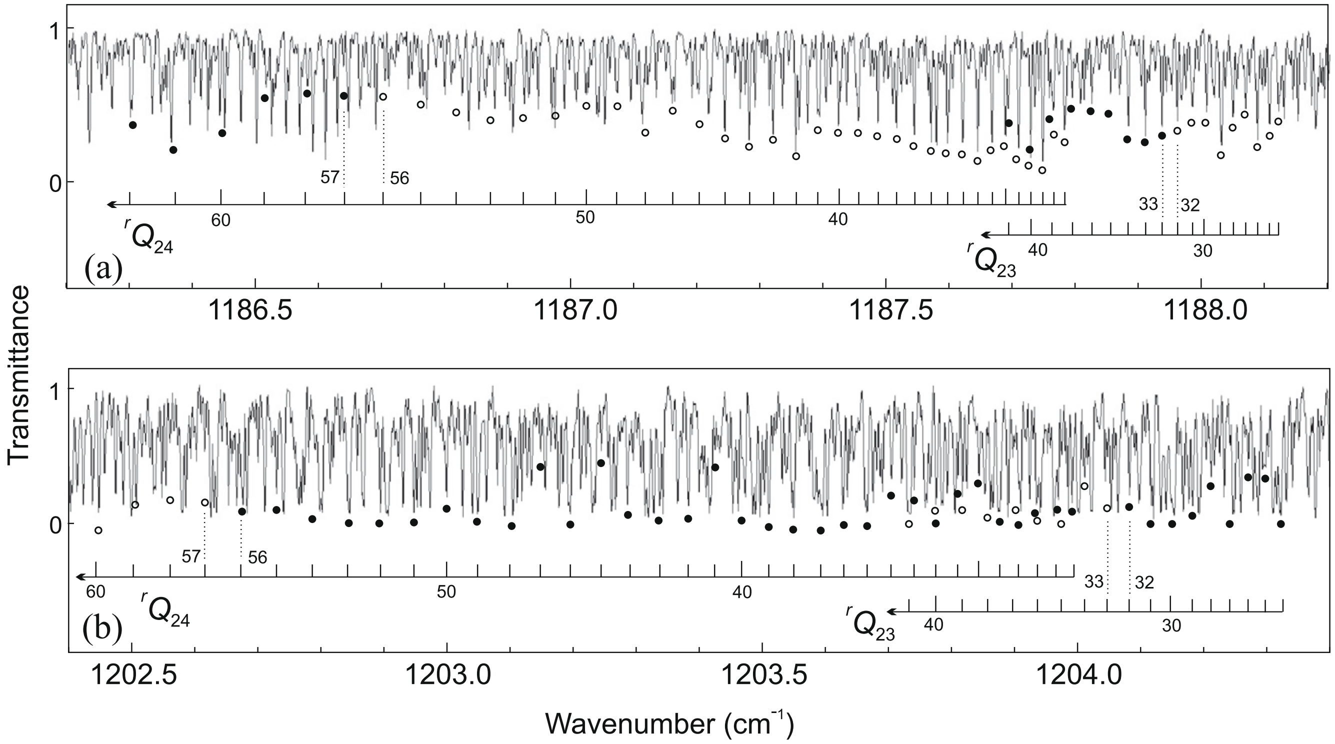

Fig. 5. Detail of the spectrum A showing the $^rQ_{23}$ and $^rQ_{24}$ branches of the $\nu_4/\nu_3+\nu_6$ band system near the Fermi crossing. Transitions assigned to the $\nu_3+\nu_6$ band are marked with full dots, transitions of the ν_4 band with empty dots. The assignment combs show some of the J quantum numbers in the ^rQ branches and indicate the positions of the level crossings.

different from all other *Q*-branches due to a larger value of the q_{22}^{36} *l*-type constant.

Although the resonance denominator $2(C - B - C\zeta)$ of the q_{22} *l*-type interaction in the $\nu_3 = \nu_6 = 1$ level is considerably larger than in the $\nu_6 = 1$ level, the intensity perturbation of the ${}^{p}Q_K$ and ${}^{r}Q_K$ branches is similar and depletes the intensities of the ${}^{p}Q_K$ branches, while intensities of the ${}^{r}Q_K$ branches are enhanced (Fig. 3b). In addition to this, the intensities of the ${}^{r}Q_K$ branches are further enhanced by the Fermi resonance, for which the intensity borrowing from the ν_4 band is stronger than for the ${}^{p}Q_K$ branches.

3.2. Hot bands in the 700 cm^{-1} region

3.2.1. The $\nu_3 + \nu_6^{\pm 1} - \nu_6^{\pm 1}$ hot band

The population of the lowest degenerate vibrational level $\nu_6 = 1$ (502.62 cm^{-1}) enables the observation of the most intense hot bands. The $2\nu_6^{\pm 2} - \nu_6^{\pm 1}$ and $2\nu_6^{0} - \nu_6^{\mp 1}$ hot bands, occurring in the ν_6 spectral region near 500 cm^{-1}, were described and analyzed in a previous study [1]. In the ν_3 region near 700 cm^{-1}, the strongest hot bands correspond to the so-called biparallel $\nu_3 + \nu_6^{\pm 1} - \nu_6^{\pm 1}$ band whose transitions follow the $\Delta l_6 = \Delta K = 0$ and $\Delta J = 0, \pm 1$ selection rules. Such bands are formed by two subbands, one with $l' = l'' = +1$ and the other with $l' = l'' = -1$; their separation follows from the slightly different $C\zeta$ values[1] in the lower and upper levels. This difference is generally due to a vibrational dependence, but in the present case the $C\zeta$ constant has an additional contribution from the Fermi resonance. Intensity enhancement due to nuclear spin statistics occurs for $K = 3p + 1$ (*p* integer) in the $l' = +1 \leftarrow l'' = +1$ subband, and for $K = 3p + 2$ in the $l' = -1 \leftarrow l'' = -1$ subband (Fig. 6a). Assignments could be performed for $4 \leqslant k''l'' \leqslant 59$ in the $l' = +1 \leftarrow l'' = +1$ subband, and for $-20 \leqslant k''l'' \leqslant -2$ in the $l' = -1 \leftarrow l'' = -1$ subband.

Besides the $\Delta l_6 = \Delta K = 0$ biparallel transitions, the spectrum in the 700 cm^{-1} region also contains perturbation-allowed transitions $\nu_3 + \nu_6^{\pm 1} - \nu_6^{\pm 1}$, following the $\Delta l_6 = \Delta K = \pm 2$ and $\Delta J = 0, \pm 1$ selection rules (Fig. 6a). This is due to the accidentally small C-B-$C\zeta$ value in the lower $\nu_6 = 1$ level, leading to strong wavefunction mixing between the q_{22} *l*-type interacting levels $|\nu_6 = 1, l_6 = -1, J, K{-}1\rangle$ and $|\nu_6 = 1, l_6 = +1, J, K + 1\rangle$. Perturbation-allowed transitions with $-56 \leqslant k''l'' \leqslant -18$ in the $l' = +1 \leftarrow l'' = -1$ subband, and with $4 \leqslant k''l'' \leqslant 22$ in the $l' = -1 \leftarrow l'' = +1$ subband, assigned from spectrum *E*, were finally assigned and included in the fit.

3.2.2. The $\nu_4^{\pm 1} - \nu_6^{\pm 1}$ difference band

Observation of difference bands of the type $\nu_i - \nu_j$[2] is generally difficult, because besides the less favorable Boltzmann factor the corresponding transition moment is small. In the case of the DCF$_3$ molecule, the *Q*-branches of the $\nu_4^{\pm 1} - \nu_6^{\pm 1}$ difference band become observable for $5 \leqslant k''l'' \leqslant 40$ (Fig. 6b), due to an intensity borrowing produced by the Fermi coupling between $\nu_4 = 1$ and $\nu_3 = \nu_6 = 1$ from the biparallel $\nu_3 + \nu_6^{\pm 1} - \nu_6^{\pm 1}$ hot band. Last but not least, the spectrum also contains some nice ${}^{s}Q_K$ branches of the "forbidden" $\nu_4^{+1} - \nu_6^{-1}$ band (Fig. 6b), observable for $-36 \leqslant k''l'' \leqslant -7$.

3.2.3. The $2\nu_3 - \nu_3$ hot band

The region of the ν_3 band around 700 cm^{-1} also contains transitions of this hot band, which has at room temperature a relative intensity of 0.035 with respect to the ν_3 fundamental band (Boltzmann factor = 0.035, degeneracy factor = 1). It is a parallel band, that resembles the ν_3 fundamental band. This hot band is not studied here but will be useful in a study of the vibrational level $\nu_3 = 2$ for which the overtone band is exceptionally weak.

4. Results and discussion

The set of the vibration-rotation data comprises more than 16,000 non-zero weighted transitions. The range of *J*/*K* values of the data, estimated experimental uncertainties and standard deviations of reproduction are summarized in Table 3. The experimental data were fitted within their experimental accuracy with a model of two vibrational levels interacting by an anharmonic Fermi resonance and two other vibration-rotation resonances described further in this section. The matrix elements of the corresponding vibration-rotation Hamiltonian used in the present analysis are summarized in Appendix A and the resulting parameters are listed in Table 4.

The two strongly interacting vibrational states are of a quite a different nature. The $\nu_3 = \nu_6 = 1$ combination level only partly carries the character of the fundamental level $\nu_6 = 1$, namely the smallness of the combination of constants C–B–$C\zeta$, which makes the pairs of levels that interact through the q_{22} *l*-type interaction quasi-degenerate. This quasi-degeneracy is removed for the levels with the strongest effects of the Fermi resonance. However, even for levels further away from the crossing, the Fermi interaction modifies effectively the value of $2(C\text{–}B\text{–}C\zeta)$ of the low-*K* levels to about 0.1 cm^{-1}, which corresponds to the observed spacing of the neighboring ${}^{p}Q_K$ and ${}^{r}Q_K$ branches around the origin of the $\nu_3 + \nu_6$ band. For the weaker q_{22} *l*-type resonance we did not need the higher-order *l*-type parameters ($q_{22}^{JJ}, q_{22}^{JK}, q_{22}^{KK}$, and f_{42}^{J}) like in the $\nu_6 = 1$ level. The parameters of the $\Delta k = \pm 6$ interaction (h_3 and h_3^{J}) could not be neglected, but varying them did not improve the fit significantly. Therefore we constrained them to the values of the vibrational ground state. The same reason holds for constraining the sextic centrifugal distortion constants H_J and H_K. Finally we fitted 11 diagonal and five off-diagonal parameters in the $\nu_3 = \nu_6 = 1$ combination level (cf. Table 4). In this case, no higher-order terms of the diagonal *z*-Coriolis interaction (τ or σ constants) were required, as they did not improve the standard deviation of the fit and were only poorly determined. It should be noted that the quartic and sextic centrifugal distortion constants are remarkably consistent with those of the ground and $\nu_6 = 1$ vibrational states [1].

The situation of the $\nu_4 = 1$ rovibrational level, if we leave the issue of the couplings with the $\nu_3 = \nu_6 = 1$ level for discussion further in this section, is somewhat different. Achieving a quantitative fit requires, in contrast to the case of $\nu_3 = \nu_6 = 1$, an inclusion of the higher-order diagonal *z*-Coriolis terms (τ and σ). Moreover, the centrifugal constants D_{JK} and D_K, and H_{KJ} and H_K to an even greater extent, have values quite different from the ground state. This is an indication of a poorer convergence of the effective Hamiltonian, probably caused by a neglected interaction, not having origin in the $\nu_3 = \nu_6 = 1$ level, because the latter does not exhibit a similar behavior. However, the source of this perturbation is not obvious because of the large separation from the nearest possible perturbing level $\nu_2 = 1$.

There is one more specific feature of the $\nu_4 = 1$ level which requires discussion in terms of the reduction of the effective vibration-rotation Hamiltonian. It is the accidental smallness of the q_{22} *l*-type interaction parameter, $q_{22}^{4} = -3.95 \times 10^{-5}$ cm^{-1}, which is a case similar to that observed in the $\nu_5 = 1$ level [9]. Although the *D*-reduction does not fail as dramatically as in the $\nu_5 = 1$ level, where the critical parameter is even smaller ($q_{22}^{5} = -1.88 \times 10^{-5}$ cm^{-1}), we have preferred to use the *Q*-reduction in the present case of $\nu_4 = 1$ (and also in the $\nu_3 = \nu_6 = 1$ level). It reduces

---

[1] The term $-2(C\zeta' - C\zeta'')K$ appears as a sum in the wavenumber expression for the $l' = +1 \leftarrow l'' = +1$ transitions, and as a difference in the corresponding expression of the $l' = -1 \leftarrow l'' = -1$ transitions.

[2] A difference band results from difference rovibrational transitions. A difference transition is a combination transition which does not start on the ground vibrational state and in which at least one vibration decreases and at least one vibration increases its degree of excitation (i.e. a transition in which more than one vibrational number changes and at least one becomes smaller).

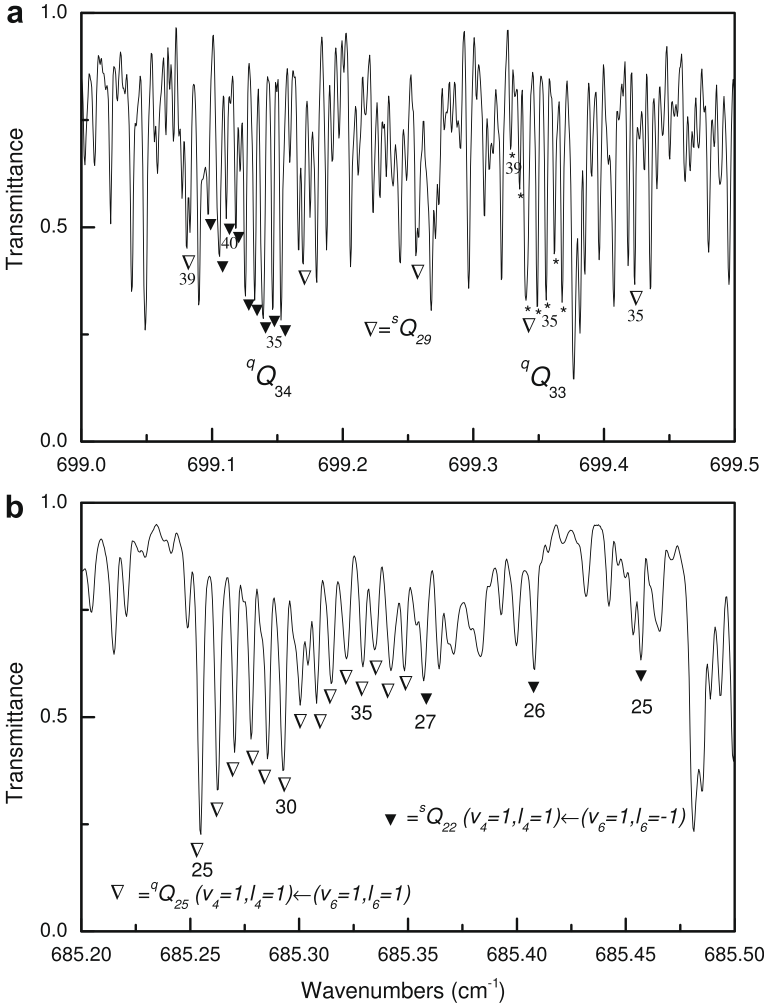

Fig. 6. (a) Detail of the spectrum *E* in the 700 cm^{-1} region, showing the $^qQ_{33}$ and $^qQ_{34}$ branches of the $\nu_3+\nu_6^{+1}-\nu_6^{+1}$ hot band, and the $^sQ_{29}$ branch of the $\nu_3+\nu_6^{+1}-\nu_6^{-1}$ perturbation-allowed hot band. (b) Detail of the spectrum *E* in the 700 cm^{-1} region, showing the $^qQ_{25}$ branch of the $\nu_4^{+1}-\nu_6^{+1}$ difference band and the $^sQ_{22}$ branch of the $\nu_4^{+1}-\nu_6^{-1}$ perturbation-allowed band.

Table 3
Summary of experimental data in the bands reaching the $\nu_3=\nu_6=1$ and $\nu_4=1$ rovibrational levels DCF$_3$.

	Range of *J*/*K*	No. of data[a]	Estimated accuracy[b]	Standard deviation[b]
$\nu_3+\nu_6$	88/70	4421	2	2.3
ν_4	75/57	9840	2	2.1
$(\nu_3+\nu_6^{\pm1})-\nu_6^{\pm1,\mp1}$	63/59	1464	2	2.5
$\nu_4^{\pm1}-\nu_6^{\pm1}$	50/40	482	2	2.3

[a] Total number of data with non-zero weights.
[b] In units of 10^{-4} cm^{-1}.

the correlations among the diagonal parameters of the $\nu_4=1$ level significantly, but has no significant effect on the anomalous values of the sextic centrifugal distortion constants mentioned above. It should also be noted that we were not able to constrain one out of the four higher-order parameters q_{22}^K, τ_J, τ_{JK}, τ_K as was suggested by Watson et al. [14], because constraining any of them led to a significantly worse reproduction of the data.

The large variety of resonance crossings between the $\nu_4=1$ and $\nu_3=\nu_6=1$ levels is a consequence of the special coincidence of their vibrational energies ($E_4>E_{36}$) and opposite signs of the $C\zeta$ constants (see Table 4). This means that the separation of levels with the same value of *K*, which are coupled by the Fermi resonance, can be estimated in the first approximation as (in units of cm^{-1})

$$E^4_{vr}-E^{36}_{vr}=E_4-E_{36}-\ 2(C\zeta_4-C\zeta_{36})\,K.l+[(C-B)_4-(C-B)_{36}]K^2 \\ +(B_4-B_{36})J(J+1)+\ \cdots\ \approx\ 14.82 \\ -0.62\,K.\,l-0.00034\,K^2+0.00020J(J+1).$$

This makes the levels with $K'\cdot l<0$ diverge from each other, while the levels with $K'\cdot l>0$ come close together. Because of the difference between their *B* constants B_4–$B_{36}>0$, the *J*-progressions of levels cross when the first line of Eq. (1) becomes negative.[3] This is the case for levels down to $K'\cdot l=+23$, as shown in the diagram of *J*-reduced energies in Fig. 7. In the subsequent lower levels with $K'\cdot l=+24$ and +25 the crossings occur between *J* = 32/33 and 56/57, respectively. For the next pair of levels $K'\cdot l=+26$ the crossing is estimated to occur at *J* = 84/85, which is beyond the range of transitions we were able to assign. It should be noted that assigning transitions to these strongly perturbed levels was not straightforward and that we had to have first

---

[3] The notion of crossing is related to the relative position of the diagonal energies before taking into account the Fermi resonance. It also corresponds to the major contribution of the basis state to the perturbed wavefunction after diagonalizing the Hamiltonian matrix with the resonance term.

Table 4
Molecular parameters of DCF_3 (in cm^{-1}) in the ground, $v_4 = 1$, and $v_3 = v_6 = 1$ vibrational levels.

Parameter	Ground state	$v_4 = 1$	$v_3 = v_6 = 1$
E	0	1211.212501 (17)	1196.389244 (17)
B	0.3309331091	0.330509471 (22)	0.330308975 (30)
C	0.18924413	0.188590222 (47)	0.188730491 (46)
$D_J \times 10^7$	3.198603	3.225899 (84)	3.17825 (13)
$D_{JK} \times 10^7$	−4.89265	−5.31074 (33)	−4.85027 (40)
$D_K \times 10^7$	2.1789	2.56944 (45)	2.15632 (48)
$H_J \times 10^{12}$	0.4745	0.4759 (10)	0.4745[a]
$H_{JK} \times 10^{12}$	−2.0065	−3.9578 (64)	−1.9480 (100)
$H_{KJ} \times 10^{12}$	2.5994	8.5324 (186)	2.5352 (147)
$H_K \times 10^{12}$	−1.0496	−5.0047 (178)	−1.0496[a]
$C\zeta$		0.16758494 (45)	−0.14367271 (35)
$\eta_J \times 10^6$		5.87582 (94)	−1.30436 (95)
$\eta_K \times 10^6$		−5.78223 (120)	1.17743 (98)
$\tau_J \times 10^{10}$		−1.0799 (31)	
$\tau_{JK} \times 10^{10}$		4.2312 (76)	
$\tau_K \times 10^{10}$		−3.0798 (86)	
$\sigma_{JK} \times 10^{13}$		1.2855 (39)	
$\sigma_{KJ} \times 10^{13}$		−2.4848 (81)	
$\sigma_K \times 10^{13}$		1.1920 (48)	
$q_{22} \times 10^4$		−0.39494 (15)	−3.07019 (15)
$q_{22}^J \times 10^9$		2.2058 (57)	2.9860 (86)
$q_{22}^K \times 10^7$		−1.0123 (13)	−0.01338 (10)
$f_{42} \times 10^9$		3.4378 (18)	−0.6162 (77)
$d_t \times 10^6$		1.3165 (14)	−0.1684 (18)
$d_t^J \times 10^{11}$		−2.0003 (79)	0.0
$h_3 \times 10^{14}$	−7.4939	−7. 4939[a]	−7. 4939[a]
$h_3^J \times 10^{19}$	4.77	4.77[a]	4.77[a]
W_{364}		8.164276 (11)	
$W_{364}^J \times 10^4$		−1.034966 (88)	
$C_{364}^x \times 10^3$		−1.0629 (41)	
$C_{364}^{x,J} \times 10^7$		−2.1506 (88)	
$d_t^{364} \times 10^7$		−1.265 (18)	

Numbers in parentheses are standard deviations in units of the last digit quoted.
[a] Constrained to the corresponding ground state values.

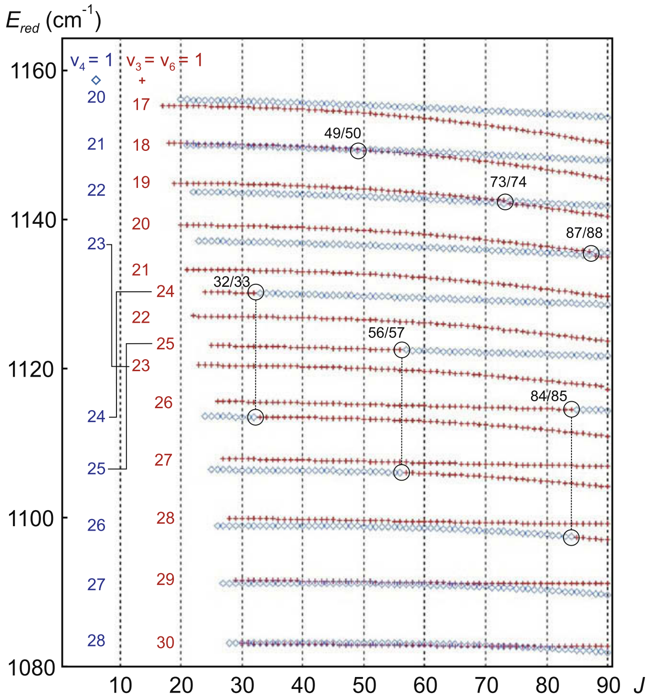

Fig. 7. J-reduced energies $E_{red} = E_{vr}(J,k,l) - B_0J(J+1) + D_J^0J^2(J+1)^2 - H_J^0J^3(J+1)^3$ around the Fermi crossing of the $v_4 = 1$ and $v_3 = v_6 = 1$ levels. Besides three crossings due to the Fermi resonance $(\Delta k = 0)$ with large displacements of levels there are also shown three crossings due to the d_t^{364} interaction $(\Delta k = 3)$. The values of J between which the crossings occur are indicated.

assigned transitions to levels with $K'{\cdot}l < 20$ and $K'{\cdot}l > 30$ and make preliminary refinement of the Fermi term W_{364}. Even when assignments of the series of transitions to the $K'{\cdot}l = +24$ and $+25$ levels were finally done, the position of the crossings (in the sense mentioned above) was changing when additional resonance terms were added to the Hamiltonian. The final value of the Fermi interaction term $W_{364} = 8.16\ cm^{-1}$ confirms the original determination from the band contour simulation which yielded $9.08 \pm 0.28\ cm^{-1}$ [4b].

Because of the described close coincidence of vibrational energies and difference of the $C\zeta$ constants, the $v_4 = 1$ and $v_3 = v_6 = 1$ levels form a kind of ‘twin’ level system in which we can find all kinds of l-type and $\Delta k = 3$ and 6 interactions which are typical for an isolated degenerate vibrational level $v_t = 1$. Therefore we are using an analogous notation of interaction constants with the only difference from the case of $v_t = 1$ being that the vibrational part of the corresponding operators of the vibration-rotation Hamiltonian $\hat{\mathbf{H}}_{vr}$ is higher by one, i.e. $v = 3$. From the survey of all crossings given in Table 5 we can see that in the studied system we can find resonance crossings with interaction terms having a selection rule for non-vanishing Hamiltonian matrix elements in the range of $\Delta k = 1, \ldots, 6$. The only interaction, for which no crossings occur, is the $\Delta k = \Delta l = \pm 2$ one. This is a consequence of an accidental coincidence of the levels with $K'{\cdot}l = 24$ and 25, for which the q_{22}^{364} term would become resonant, with those for which the Fermi resonance already occurs. The much stronger Fermi resonance displaces these levels dramatically, as shown in Fig. 7, so that the weaker $\Delta k = \Delta l = \pm 2$ interaction is tuned out of resonance.

With the use of these coupling terms, the reduction of the interaction Hamiltonian comes into question. The reduction problem in the system of vibrational states $v_n = 1$, $v_t = 1/v_{t'} = 1$ with a Fermi resonance has been studied recently by Nová-Stříteská et al. [15]. From there it follows that four (out of seven) parameters of the interaction Hamiltonian $\hat{\mathbf{H}}_{int} = \hat{\mathbf{H}}_{30} + \hat{\mathbf{H}}_{31} + \hat{\mathbf{H}}_{32}$ can be varied in the fits because of three free parameters of the contact transformation. Out of these four adjustable parameters, the two lowest-order Fermi and Coriolis coupling terms cannot be removed by the contact transformation and have to be fitted. The third parameter that was always varied in our fits was the J-dependent terms of the Fermi coupling. Of the remaining four interaction parameters then only one more can be fitted and the remaining three have to be constrained. We have tested all these possibilities in our fits. Fitting of the K-dependent term of the Fermi coupling or the $\Delta k = 0$ Coriolis-type interaction (Eq. (A8)) term lead to strong correlations and at the same time to an unsatisfactory reproduction of the data. The fits provided quantitative reproduction of the data when one of the q_{12}^{364} or q_{22}^{364} constants was varied. We achieved even a slightly better fit as for the interaction parameter errors and correlations by fitting the d_t^{364} term from the higher-order interaction Hamiltonian $\hat{\mathbf{H}}_{33}$ as the fourth interaction term instead of the remaining fourth parameter from $\hat{\mathbf{H}}_{32}$. We may explain this somewhat higher significance of the higher-order term over the lower-order ones by the observed resonant crossings of levels coupled by the $\Delta k = \pm 3$ interaction whereas the q_{22}^{364} interaction is tuned out from resonance by the coincidence with the Fermi crossing and the q_{12}^{364} term is an additional contribution to the Coriolis resonance whose crossing is observed only for a single and high value of K. We slightly favor the fit with d_t^{364} because it also provides a better consistency of the d_t^{36} and d_t^{6} constants. We present the resulting set of parameters in Table 4 while the constants from the two other fits (with q_{12}^{364} or q_{22}^{364} varied) are included for comparison in the associated supplementary data (Appendix B). It should be noted that any of these sets of interaction parameters was sufficient for the accurate description of all other resonances with $\Delta k \geqslant 4$.

Table 5
Resonant crossings in the system of the $v_3 = v_6 = 1$ and $v_4 = 1$ rovibrational levels of DCF$_3$.

Resonance parameter	$\lvert\Delta k\rvert$	$\langle k^l \rvert$	$\lvert k^l \rangle$	Crossing J
$\langle v_{36}\rvert W_{364} \lvert v_4\rangle$				
	0	24^{+1}	24^{+1}	**32/33**[a]
		25^{+1}	25^{+1}	**56/57**
		26^{+1}	26^{+1}	(84/85)
$\langle v_{36}\rvert C^x_{364} \lvert v_4\rangle$				
	1	55^{-1}	54^{+1}	(77/78)
		56^{-1}	55^{+1}	(70/71)
$\langle v_{36}\rvert q^{364}_{22} \lvert v_4\rangle$				
	2	$22, 23^{-1}$	$24, 25^{+1}$	No crossing
$\langle v_4\rvert d^{364}_t \lvert v_{36}\rangle$				
	3	18^{+1}	21^{+1}	**49**/50
		19^{+1}	22^{+1}	(73/74)
		20^{+1}	23^{+1}	(87/88)
$\langle v_{36}\rvert f^{364}_{42} \lvert v_4\rangle$				
	4	22^{+1}	26^{-1}	72/73
$\langle v_{36}\rvert f^{364}_{52} \lvert v_4\rangle$				
	5	17^{+1}	12^{-1}	69/70
$\langle v_{36}\rvert h^{364}_3 \lvert v_4\rangle$				
	6	8^{+1}	14^{+1}	45/46
		15^{-1}	21^{-1}	50/51
$\langle v_{36}\rvert q^6_{12} \lvert v_{36}\rangle$				
	1	2^{-1}(A$_-$)	1^{+1}(A$_-$)	**33/34**
		3^{-1}	2^{+1}	**44/45**
		4^{-1}	3^{+1}	52/53
		5^{-1}	4^{+1}	60/61
		6^{-1}	5^{+1}	66/67
		7^{-1}	6^{+1}	73/74
$\langle v_{36}\rvert d^{36}_t \lvert v_{36}\rangle$				
	3	1^{-1}	-2^{-1}	**16/17**
$\langle v_{36}\rvert h^{36}_3 \lvert v_{36}\rangle$				
	6	-2^{-1}	4^{-1}	56/57
$\langle v_4\rvert q^4_{12} \lvert v_4\rangle$	1	1^{+1}(A$_+$)	2^{-1}(A$_+$)	**46/47**
$\langle v_4\rvert h^4_3 \lvert v_4\rangle$	6	-2^{-1}	4^{-1}	59/60

[a] Values of J in boldface denote crossings where the transitions right below and above the crossing were assigned in the spectrum. Numbers in parentheses are estimated positions of crossings where data around them were not assigned.

Besides these vibration-rotation resonances between the two vibrational levels, which are spread over the whole range of studied K values, we also observed effects of the q_{12}/d_t resonances at low values of K in both vibrational levels, which are typical for the oblate symmetric top molecules. The diagram of J-reduced levels in Fig. 8 shows the situation in the $v_3 = v_6 = 1$ level with the whole series of resonant crossings. Two of them occurring for the lowest J and K values are due to the d_t resonance, while the rest are due to the q_{12} resonance. It should be noted, that even though resonances with both types of coupling terms (q_{12} and d_t) are observed, the fit has to be performed with one of the parameters constrained (the Q-reduction in the present case) as a result of the reduction theory.

In the $v_4 = 1$ level with a different combination of the C-B-$C\zeta$ constants, only one resonance crossing due to the q^4_{12} or d^4_t term occurs, namely between the A$_+$ components of the $kl = +1$ and $kl = -2$ levels. This interaction can produce perturbation-allowed transitions and we were indeed able to assign 31 of them in the $^sP_0$ and $^sR_0$ branches and 22 in the $^oP_3$ and $^oR_3$ branches of the v_4 band. Although analogous crossings were found in the $v_3 = v_6 = 1$ level, we found only a few weak lines that might correspond to perturbation-allowed transitions. We can explain the absence of convincing systematic series of lines by the much weaker d_t coupling term in the $v_3 = v_6 = 1$ level, which makes the intensities of the perturbation-allowed transitions in the latter band weaker by about two orders of magnitude. Because of their marginal effect on the fit, these transitions were not included in the analysis.

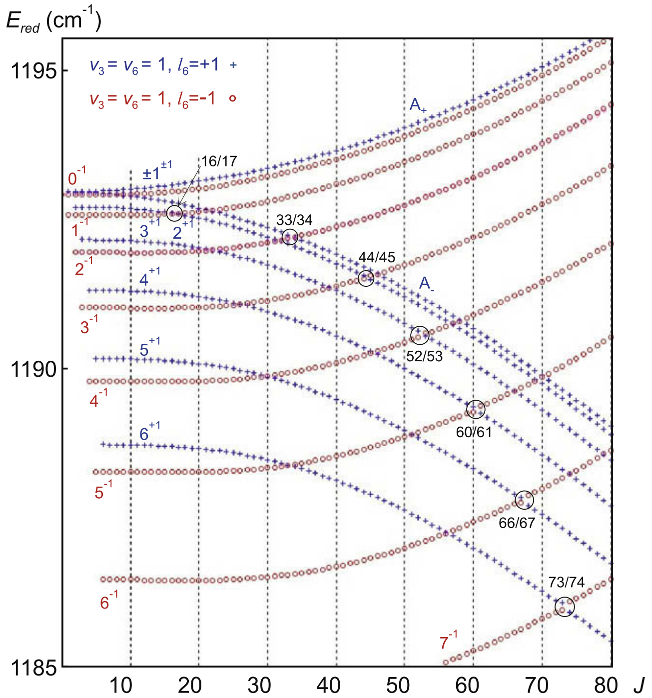

Fig. 8. J-reduced energies of the lowest K levels in the $v_3 = v_6 = 1$ vibrational state. The indicated resonance crossings are due to the d^{36}_t and q^{36}_{12} interactions. The values of J between which the crossings occur are indicated.

The analysis of the $v_3 + v_6$ combination band, together with the earlier analyses of the v_3 and v_6 fundamental bands, provide the anharmonicity constant $x_{36} = E_{36} - E_3 - E_6 = -0.517420\,(21)\ \mathrm{cm}^{-1}$.

For the least-squares fitting, the data were given weights proportional to the inverses of their estimated experimental uncertainties. It was a very frequent case in the congested spectra that these had to be individually increased in cases of line overlaps, which were indicated by significant discrepancies in the LSCD checking. We finally achieved a quantitative reproduction of all experimental data in the whole range of rotational states.

5. Conclusions

The present work concludes the high-resolution studies of the fundamental bands of deuterated fluoroform by the analysis of the vibrational level $v_4 = 1$. The close coincidence with the $v_3 = v_6 = 1$ combination level required their theoretical treatment as of vibrational states coupled by an anharmonic Fermi and Coriolis resonances as well as higher-order resonance terms in order to describe correctly the large number of local level crossings. This study provides vibrational energies and rotational constants deperturbed from effects of these resonances which are important for improving the information on the molecular force field and for studies of higher excited levels of this molecule.

Acknowledgments

The support from the Grant Agency of the Academy of Sciences of the Czech Republic (Project No. IAA400400706) and the Ministry of Education, Youth and Sports of the Czech Republic (research program LC06071) are gratefully acknowledged. A. Predoi-Cross is grateful for financial support from the National Sciences and

Engineering Research Council of Canada (NSERC). The authors would like to thank the authors of Ref. [15] for communicating their results prior to publication.

Appendix A. Definition of matrix elements of the effective vibration–rotation Hamiltonian

The diagonal matrix elements up to seventh order were taken as

$$\begin{aligned}E_{vr}(J,k,l) = {} & E_v + B_v J(J+1) + (C_v - B_v)k^2 - D_J^v J^2(J+1)^2 \\ & - D_{JK}^v J(J+1)k^2 - D_K^v k^4 + H_J^v J^3(J+1)^3 + H_{JK}^v J^2(J+1)^2 k^2 \\ & + H_{KJ}^v J(J+1)k^4 + H_K^v k^6 + \Big[-2C\zeta_v + \eta_J^v J(J+1) + \eta_K^v k^2 \\ & + \tau_J^v J^2(J+1)^2 + \tau_{JK}^v J(J+1)k^2 + \tau_K^v k^4 + \sigma_J^v J^3(J+1)^3 \\ & + \sigma_{JK}^v J^2(J+1)^2 k^2 + \sigma_{KJ}^v J(J+1)k^4 + \sigma_K^v k^6\Big]\, kl \qquad \text{(A1)}\end{aligned}$$

The diagonal z-Coriolis term $C\zeta_v$ (and its expansion η, τ, and σ-terms) vanish for the ground vibrational state.

In the $v_4 = 1$ and $v_3 = v_6 = 1$ vibrational levels the following l-type operators were taken into account

$$\begin{aligned}&\langle v_t^{l\pm2}; J, k\pm2 \mid (\mathbf{H}_{22} + \mathbf{H}_{24})\,/hc \mid v_t^{l}; J, k\rangle \\ &\quad = [(v_t \mp l_t)\,(v_t \pm l_t + 2)]^{1/2}\,\{\, q_{22} + f_{22}^J J(J+1) \\ &\qquad + f_{22}^K[\,k^2 + (k\pm2)^2]\,\}\, F_2^{\pm}(J,k) \qquad \text{(A2)}\end{aligned}$$

$$\begin{aligned}&\langle v_t^{l_t\pm2}; J, k\mp4 \mid \mathbf{H}_{24}\,/hc \mid v_t^{l_t}; J, k\rangle \\ &\quad = [(v_t \mp l_t)\,(v_t \pm l_t + 2)]^{1/2} f_{42}\, F_4^{\mp}(J,k) \qquad \text{(A3)}\end{aligned}$$

Because of the accidental smallness of the q_{22} term in the $v_4 = 1$ level we used the effective Hamiltonian in the Q-reduction (with the constraint $q_{12}^4 = 0$). In the $v_3 = v_6 = 1$ vibrational level there was not such a problem and the two reductions Q and D were equivalent. We thus used the Q-reduction in both studied levels with the matrix elements of the operator describing the $\Delta k = \pm3$ interaction in the form

$$\begin{aligned}&\langle v_t^{l_t}; J, k\pm3 \mid (\mathbf{H}_{23} + \mathbf{H}_{25})/hc \mid v_t^{l_t}; J, k\rangle \\ &\quad = [d_t + d_t^J J(J+1)]\; l_t\, F_3^{\pm}(J,k) \qquad \text{(A4)}\end{aligned}$$

The matrix elements of the operator of the $\Delta k = \pm6$ interaction

$$\begin{aligned}&\langle v_t^{l_t}; J, k\pm6 \mid (\mathbf{H_{06}} + \mathbf{H_{08}})/hc \mid v_t^{l_t}; J, k\rangle \\ &\quad = [h_3 + h_3^J J(J+1)]\; F_6^{\pm}(J,k) \qquad \text{(A5)}\end{aligned}$$

were included in the vibrational ground state and in the $v_4 = 1$ and $v_3 = v_6 = 1$ levels.

In the description of the interaction Hamiltonian $\hat{\mathbf{H}}_{int} = \hat{\mathbf{H}}_{30} + \hat{\mathbf{H}}_{31} + \hat{\mathbf{H}}_{32}$ we used the names of parameters analogous to the case of an isolated degenerate vibrational level $v_t = 1$. The correspondence to the parameters of Ref. [15] is given by the explicit form of the individual Hamiltonian terms $\hat{\mathbf{H}}_{vr}$ in the following equations.

The Fermi interaction between the $v_4 = 1$ and $v_3 = v_6 = 1$ levels was described by the matrix element

$$\begin{aligned}&\left\langle v_3 = 1, v_6 = 1^{\pm1}, v_4 = 0^0, J, k \middle| \left(\mathbf{H}_{30} + \mathbf{H}_{32}^{J,K}\right)/hc \middle| v_3 = 0, v_6 = 0^0, v_4 = 1^{\pm1}, J, k\right\rangle \\ &\quad = W_{364} + W_{364}^J J(J+1) + W_{364}^K k^2 \qquad \text{(A6)}\end{aligned}$$

The ($\Delta k = \pm1$, $\Delta l = \mp2$) Coriolis-type interaction was considered as

$$\begin{aligned}&\left\langle v_3 = 1, v_6 = 1^{\pm1}, v_4 = 0^0,\; J, k\mp1 \middle| (\mathbf{H}_{31}^x + \mathbf{H}_{33}^x)/hc \right. \\ &\left.\middle| v_3 = 0, v_6 = 0^0, v_4 = 1^{\mp1},\; J, k\right\rangle \\ &\quad = \pm2\,[C_{364}^x + C_{364}^{x,J} J(J+1) + C_{364}^{x,K}\, k^2]\, F_1^{\mp}(J,k) \qquad \text{(A7)}\end{aligned}$$

and the ($\Delta k = 0$, $\Delta l = 0$) Coriolis-type interaction as

$$\begin{aligned}&\left\langle v_3 = 1, v_6 = 1^{\pm1}, v_4 = 0^0, J, k \middle| \mathbf{H}_{31}^z/hc \middle| v_3 = 0, v_6 = 0^0, v_4 = 1^{\pm1}, J, k\right\rangle \\ &\quad = \pm2\,C_{364}^z\, k \qquad \text{(A8)}\end{aligned}$$

There is another ($\Delta k = \pm1$, $\Delta l = \mp2$) interaction term analogous to the q_{12} term

$$\begin{aligned}&\left\langle v_3 = 1, v_6 = 1^{\pm1}, v_4 = 0^0, J, k\mp1 | H_{32}^{xz}/hc | v_3 = 0, v_6 = 0^0, v_4 = 1^{\mp1}, J, k\right\rangle \\ &\quad = 2q_{12}^{364}\,(2k\mp1)F_1^{\mp}(J,k) \qquad \text{(A9)}\end{aligned}$$

The ($\Delta k = \pm2$, $\Delta l = \pm2$) interaction term was taken as

$$\begin{aligned}&\left\langle v_3 = 1, v_6 = 1^{\pm1}, v_4 = 0^0, J, k\pm2 \middle| \mathbf{H}_{32}^{xy}/hc \middle| v_3 = 0, v_6 = 0^0, v_4 = 1^{\mp1}, J, k\right\rangle \\ &\quad = 2\,q_{22}^{364}\, F_2^{\pm}(J,k) \qquad \text{(A10)}\end{aligned}$$

The matrix elements of the $\Delta k = \pm3$ interaction were taken as

$$\begin{aligned}&\left\langle v_3 = 1, v_6 = 1^{\pm1}, v_4 = 0^0, J, k\pm3 \middle| \mathbf{H}_{33}/hc \middle| v_3 = 0, v_6 = 0^0, v_4 = 1^{\pm1}, J, k\right\rangle \\ &\quad = d_t^{364} l_t\, F_3^{\pm}(J,k) \qquad \text{(A11)}\end{aligned}$$

The sign in $k \pm 3$ does not correlate with the signs of the l_t quantum numbers. One can thus use either l_6 or l_4 for l_t in the right hand side of Eq. (A11).

The notation of the matrix elements of rotational shifting operators was taken conventionally as

$$F_n^{\pm}(J,k) = \prod_{i=1}^{n} [J(J+1) - (k \pm i \mp 1)(k \pm i)]^{1/2} \qquad \text{(A12)}$$

Appendix B. Supplementary data

Supplementary data associated with this article are available on ScienceDirect (www.sciencedirect.com), as part of the Ohio State University Molecular Spectroscopy Archives (http://msa.lib.ohio-state.edu/jmsa_hp.htm), and in the online version, at doi:10.1016/j.jms.2009.09.007.

References

[1] P. Pracna, A. Ceausu-Velcescu, H. Bürger, J. Mol. Spectrosc. 250 (2008) 59–69, doi:10.1016/j.jms.2008.04.011.

[2] J. Breidung, J. Cosléou, J. Demaison, K. Sarka, W. Thiel, Mol. Phys. 102 (2004) 1827–1841.

[3] H.-R. Dübal, M. Lewerenz, M. Quack, J. Chem. Phys. 85 (1986) 34–39.

[4] (a) A. Ruoff, H. Bürger, S. Biedermann, Spectrochim. Acta A 27A (1971) 1359–1376;
(b) A. Ruoff, H. Bürger, S. Biedermann, R. Anttila, Spectrochim. Acta A 31A (1975) 1099–1100.

[5] N.J. Fyke, P. Lockett, J.K. Thompson, P.M. Wilt, J. Mol. Spectrosc. 58 (1975) 87–101.

[6] C.C. Costain, J. Mol. Spectrosc. 9 (1962) 317–336.

[7] P. Pracna, Š. Urban, F. Kolář, J. Cosléou, J. Demaison, P. Paplewski, H. Bürger, J. Mol. Struct. 517–518 (2000) 119–126.

[8] R. Bocquet, D. Boucher, W.D. Chen, D. Papoušek, G. Wlodarczak, J. Demaison, J. Mol. Spectrosc. 163 (1994) 291–299.

[9] P. Pracna, K. Sarka, J. Demaison, J. Cosléou, F. Herlemont, M. Khelkhal, H. Fichoux, D. Papoušek, M. Paplewski, H. Bürger, J. Mol. Spectrosc. 184 (1997) 93–105.

[10] H. Bürger, J. Cosléou, J. Demaison, C. Gerke, H. Harder, H. Mäder, M. Paplewski, D. Papoušek, K. Sarka, J.K.G. Watson, J. Mol. Spectrosc. 182 (1997) 34–49.

[11] (a) G. Guelachvili, K. Narahari Rao, Handbook of Infrared Standards, Academic Press, San Diego, 1986;
(b) G. Guelachvili, M. Birk, Ch.J. Bordé, J.W. Brault, L.R. Brown, B. Carli, A.R.H. Cole, K.M. Evenson, A. Fayt, D. Hausamann, J.W.C. Johns, J. Kauppinen, Q. Kou, A.G. Maki, K. Narahari Rao, R.A. Toth, W. Urban, A. Valentin, J. Vergès, G. Wagner, M.H. Wappelhorst, J.S. Wells, B.P. Winnewisser, M. Winnewisser, Pure Appl. Chem. 68 (1996) 193–208;
(c) G. Guelachvili, M. Birk, Ch.J. Bordé, J.W. Brault, L.R. Brown, B. Carli, A.R.H. Cole, K.M. Evenson, A. Fayt, D. Hausamann, J.W.C. Johns, J. Kauppinen, Q. Kou, A.G. Maki, K. Narahari Rao, R.A. Toth, W. Urban, A. Valentin, J. Vergès, G. Wagner, M.H. Wappelhorst, J.S. Wells, B.P. Winnewisser, M. Winnewisser, J. Mol. Spectrosc. 177 (1996) 164–179;
(d) G. Guelachvili, M. Birk, Ch.J. Bordé, J.W. Brault, L.R. Brown, B. Carli, A.R.H. Cole, K.M. Evenson, A. Fayt, D. Hausamann, J.W.C. Johns, J. Kauppinen, Q. Kou,

A.G. Maki, K. Narahari Rao, R.A. Toth, W. Urban, A. Valentin, J. Vergès, G. Wagner, M.H. Wappelhorst, J.S. Wells, B.P. Winnewisser, M. Winnewisser, Spectrochim. Acta A 52A (1996) 717–732.
[12] L.S. Rothman, D. Jacquemart, A. Barbe, D. Chris Benner, M. Birk, et al., JQSRT 96 (2005) 139–204.
[13] W. Lodyga, M. Kreglewski, P. Pracna, Š. Urban, J. Mol. Spectrosc. 243 (2007) 182–188, doi:10.1016/js.2007.02.004.
[14] J.K.G. Watson, C. Gerke, H. Harder, K. Sarka, J. Mol. Spectrosc. 187 (1998) 131–141.
[15] L. Nová-Stříteská, K. Sarka, Š. Urban, J. Mol. Spectrosc. 257 (2009) 108–110.